Adsorption properties, the pH-sensitive release of 5-fluorouracil and cytotoxicity studies of mesoporous silica drug delivery matrix

Eva Beňová, David Bergé-Lefranc, Vladimír Zeleňák, Miroslav Almáši, Veronika Huntosova, Virginie Hornebecq

Adsorption properties, the pH-sensitive release of 5-fluorouracil and cytotoxicity studies of mesoporous silica drug delivery matrix

Eva Beňová[a,b], David Bergé-Lefranc[c], Vladimír Zeleňák[a,*], Miroslav Almáši[a], Veronika Huntošová[d], Virginie Hornebecq[b,*]

[a] Department of Inorganic Chemistry, Faculty of Science, P.J. Šafárik University, Moyzesova 11, SK-041 54 Košice, Slovakia
[b] Aix Marseille Univ, CNRS, MADIREL, Marseille, France
[c] Aix Marseille Univ, CNRS, IMBE, Faculté de Pharmacie, Marseille, France
[d] Center for Interdisciplinary Biosciences, Technology and Innovation Park, P. J. Šafárik University in Košice, Jesenna 5, 041 54 Košice, Slovakia

A B S T R A C T

Mesoporous silica materials were investigated as the carriers for pH-sensitive drug delivery systems. Porous silica SBA-15 was first functionalized by anchoring N-[3-(trimethoxysilyl) propyl] aniline groups on the surface. After loading of an antineoplastic agent 5-fluorouracil, the pores were capped by β-cyclodextrin molecules. The studied samples were characterized by N_2 adsorption/desorption measurements, thermal analysis, powder X-Ray Diffraction, and Transmission Electron Microscopy. Adsorption properties of 5-fluorouracil were explored *via* the construction of adsorption isotherms. The amount of 5-FU adsorbed on amine-functionalized SBA-15 was 60 mg per 1 g of solid. The adsorption of 5-fluorouracil on silica was also monitored by microcalorimetry, showing low adsorption enthalpies. Drug release properties from matrices were studied using UV–Visible spectroscopy with the un-blocked and blocked pores configuration to demonstrate the efficiency of the pH-responsive nanovalves and evaluated using different kinetic models. It was shown that no drug release occurred at neutral pH and that more than 80% of drug adsorbed amount was released at pH = 5. Working at the equilibrium, the initial burst of the drug from the silica surface, usually observed in other porous silica drug delivery systems, was avoided. The interaction between the β-cyclodextrin molecules and grafted amine functions were also studied as a function of pH. Finally, the cytotoxicity tests were performed using human glioma U87 MG cells.

1. Introduction

The unfavorable physicochemical properties of many drug compounds affect their bioavailability and consequently the pharmacokinetic efficiency of the medical treatment. For example, drug molecules with a lack of specificity and solubility lead patients to take high doses of the drug to achieve sufficient therapeutic effects. This is a leading cause of adverse drug reactions, particularly for drugs with a narrow therapeutic window or cytotoxic chemotherapeutics [1]. Lack of specificity of a drug molecule leads to the high-dosage regimen and cause undesired interactions of a drug with healthy tissues or cells [2]. The possible solution to overcome these problems is to design the efficient Drug Delivery Systems (DDSs) that enable to control the rate, time, and place of drugs release in the body [3]. The DDSs improve the pharmacological properties of drug molecules by modifying their pharmacokinetic profile, solubility and bio-distribution [4]. Among structurally stable materials that have been investigated, mesoporous silica materials (MSMs) have become apparent as a promising drug vehicle due to their unique mesoporous structure that preserves a level of chemical stability, surface functionality, and biocompatibility. The MSMs have been used for delivery of a variety of drug molecules, e.g.: chemotherapeutics agents [5–7], antibiotics [8,9], antimicrobial drugs [10], anti-inflammatory molecules [11–14]. One of their main advantages is their ability to be used for both hydrophilic active agents and poorly water-soluble drugs by increasing their solubility [15]. For example, Mellaerts *et al.* reported the increase of the oral bioavailability of the poorly water-soluble drug, itraconazole using mesoporous silica nanoparticles as drug delivery agents [16].

Another advantage of porous silica drug delivery system is the possibility to design zero-premature cargo release nanosystems by blocking the pore openings using various gatekeepers [17–19]. Lately, most of the research effort for drug delivery has been committed to cancer therapy and internal stimuli such as pH, redox potential, enzymes, etc. that are typical of the treated pathology [20–22]. pH-

responsive MSMs have attracted extensive research interest because cancer cells cause the decrease of pH environment to more acidic values compared to the pH environment of healthy cells, which provides an efficient way to control the drug release behavior by pH variations [23,24]. There are many strategies to construct pH-responsive drug delivery systems, e.g. using polyelectrolyte gatekeepers [25], pH-sensitive linkers (such as acetal bond, hydrazine bond, ester bond) [26], acid-decomposable inorganic gatekeepers [27] and supramolecular nanovalves [28]. The latter includes an immobilized stalk molecule covalently attached to silica surface and a mobile cyclic molecule encircling the stalk via non-covalent interactions [29]. A lot of cucurbituril and cyclodextrin (CD) molecules have been demonstrated to be effective supramolecular pore gatekeepers for mesoporous silicas [30,31]. Particularly for CD, different molecules were grafted on the porous silica surface and then tested as pH-responsive gatekeepers. Meng *et al.* reported a novel MSM delivery system for doxorubicin, a chemotherapeutic agent, based on β-cyclodextrin nanovalves testing different aromatic amines. Best results were obtained using N-methylbenzimidazole as stalks with a maximum release percentage of 40% in acidic conditions (pH = 5) [32]. The delivery of doxorubicin was also tested in the work of Bai *et al.* who constructed a controlled release system using p-anisidine stalks. Even if the pH-dependency of release properties were successfully studied for short release time (< 6 h), the loading efficiency of doxorubicin was very low (4,5%), that represented 2.44 mg of doxorubicin per 1 g of silica support [33].

Considering silica DDSs, several important parameters have to be optimized all together both in terms of loading and release properties. In this way, the loading efficiency i.e. the amount of available drug that is incorporated in and only in the porous volume should be as high as possible and the release profile in time should be as progressive as possible, avoiding the burst effect. Therefore, in the present paper, both adsorption and pH-sensitive release properties of a model drug on mesoporous silica material SBA-15 were studied and optimized in this context. The antineoplastic agent 5-fluorouracil (5-FU), that is a first-line anti-cancer drug, commonly used to treat colorectal, gastrointestinal and breast cancer, was employed as a drug molecule in our study. However, the efficiency of 5-FU is limited by high rate of metabolism in the body, short biological half-life, non-uniform oral adsorption and cytotoxicity. To be effective it has to be administrated at higher concentrations or more frequent doses. In this work, we assume that its encapsulation in a host delivery system can reduce the frequency of dosing or it could help the drug to be more effective even at lower concentrations.

In our DDSs, supramolecular nanovalves based on β-CD units were used as gatekeeper and three different amines were grafted onto the mesoporous silica surface and used as stalk molecules. For the grafting, we have used aliphatic amines namely propylamine (AP), tetraethylenepentamine (TEPA) aromatic amine propyl aniline (N-ANI). Our study showed, that the DDSs based on studied aliphatic amines and β-cyclodextrin molecules do not work effectively and showed poor tightness and premature drug release (see Supporting information, Fig. S1). The more promising results were obtained using a gatekeeper system composed of aromatic propyl aniline based stalk (N-ANI) and β-CD units, which properties are described in the present study. It is note, that combination of N-ANI ligands and β-CD molecules in construction of pH-responsive DDSs have been already reported [34,35]. However, in our study adsorption properties of drug were studied on pure silica matrix and functionalized one from a thermodynamic point of view. Moreover, the construction of adsorption isotherms and their modeling as well as the determination of enthalpies of adsorption using calorimetric measurements were realized. As far as our knowledge, such an extensive study concerning thermodynamic description has not been reported in the literature yet. Moreover, the cytotoxicity of the prepared DDS using U87 MG cancer cells complete our study.

2. Experimental section

All chemicals used in the syntheses were obtained by Sigma-Aldrich and Across Organics companies in the highest purities and used without further purification. Anhydrous solvents were obtained after standard procedures described in the literature [36] and stored over molecular sieves.

2.1. Synthesis and functionalization mesoporous silica SBA-15

The synthesis of porous silica was carried out according to the procedure reported in [37]. 4 g of triblock copolymer P_{123}, (Poly (ethylene glycol)-block-poly(propylene glycol)-block-poly(ethylene glycol)) was dissolved in 30 g of distilled water at T = 308 K under high acidic conditions produced by the addition of 120 g of HCl (2 M). The mixture was stirred until it became homogenous. Then, 8.5 g of TEOS was added dropwise to the solution followed by continuous stirring for 20 h at T = 308 K. After this time, the solution was aged at 80 °C for 24 h. The white solid product was filtered off, washed with distilled water and dried at room temperature.

Porous SBA-15 matrix was obtained by calcination of as-synthesized SBA-15 in airflow at 600 °C. The calcination procedure was as follows: the sample was heated to 150 °C with a heating rate 3 °C/min and the sample was held at this temperature for 3 h. Subsequently, the temperature was increased to 600 °C by the rate 1 °C/min and the sample was held at this temperature for 7 h. In the last step, the sample was cooled down to room temperature.

The surface modification (functionalization) of silica was carried out by a post-synthetic grafting procedure. Typically, 1 g of calcined SBA-15 was dispersed in anhydrous toluene, mixed with 3 mL of N-[3-(trimethoxysilyl) propyl] aniline (12,5 mmol) and refluxed under N_2 for 20 h. The obtained product was centrifuged, several times washed with toluene and ethanol and dried at T = 313 K for 24 h. The material was denoted as SBA-15_N-ANI.

2.2. Drug loading and pores capping

5-fluorouracil (5-FU) was taken as a model drug to estimate the loading and release performance from both SBA-15 and SBA-15_N-ANI. Various information concerning the solubility of 5-FU in water are reported in the literature, i.e.: 5 mg/ml [38], 8.62 mg/ml [39], 12 mg/ml [40]. Since the drug 5-FU is sparingly soluble in the water, the upper concentration limit of 5-FU in our experiments was set to 6.5 mg/ml.

2.2.1. Adsorption experiments

Adsorption isotherm experiments were carried out using a solution depletion method. The experimental process consisted in the following steps: 20 mg of samples were dispersed in a series of plastic vials containing 2 mL of 5-FU aqueous solution with different initial concentrations (from 0.1 to 6.5 mg/ml). Then, the adsorption process was carried out, with continuous stirring, at T = 310 K for 24 h to ensure equilibrium. The separation of a solid phase from the supernatant liquid was achieved by centrifugation at 10 000 rpm (corresponding to a relative centrifugal force of 7400 g) for several minutes. The supernatant was then analyzed by using UV–Vis spectroscopy (wavelength range 200 – 350 nm) to determine the equilibrium concentration of 5-Fu (C_{eq}) at the maximum of the absorption band (λ = 266 nm). Prior to the determination of the concentration of 5-FU, a calibration curve has been established based on solutions with different concentrations of 5-FU (see Fig. S2 in the Supplementary information). The linearity of the calibration curve was confirmed by the correlation coefficient $R^2 = 0.99996$. Then, the amount adsorbed, Q_{ADS} was calculated as follows:

$$Q_{ADS} = \frac{V(C_i - C_{eq})}{m_s} \quad (1)$$

where C_i is the initial concentration in mol·dm^{-3} (abbreviation M), C_{eq} is the equilibrium concentration (M), V is the volume of the drug solution (dm^3 or L), and m_s is the mass of adsorbent used (g).

Microcalorimetric experiments were performed on TAM 2277 microcalorimeter in order to determine the adsorption enthalpies. During these experiments, solids (SBA-15 and SBA-15_N-ANI) were maintained in water suspension using a stirring system and a stock solution of 5-FU was added by 5 μL aliquots step by step (20 injections). Next, the heat flow peaks were time-integrated and after correction of dilution effects, the integral enthalpies were obtained.

2.2.2. Preparation of β-CD capped SBA-15_N-ANI_5-FU material

A solution of 5-FU (6,5 mg/ml) was prepared in distilled water at room temperature. Then, 100 mg of the SBA-15_N-ANI and 10 mL of 5-FU solution were mixed and stirred at T = 310 K until the mesoporous silica stopped adsorbing the drug, which was monitored by UV–Vis absorption spectroscopy. It was found that 24 h of the adsorption process was sufficient to achieve equilibrium. Then, the pH of the solution was adjusted to 7.4 with the addition of NaOH solution (1 M) and 600 mg of β-CD was added to the mixture and stirred overnight at T = 310 K. The 5-FU-loaded β-CD-capped mesoporous silica was washed with water with pH adjusted to 7.4 by the same NaOH solution, centrifuged and used in further experiments.

2.3. Drug release experiments

The experiments involving 5-FU release by sample SBA-15_N-ANI were performed by two different procedures. For both, the adsorption of 5-FU and pores capping were carried out first as described above. In both cases, the mixtures were stirred at 37 °C in a tube rotator. The release amount of 5-FU was calculated from a standard curve using UV–Vis spectroscopy at λ = 266 nm.

1st procedure: after adsorption of 5-FU and pores blocking using β-CD molecules, the suspension was centrifuged and the supernatant was removed to recover the solid phase. Then, 100 mg of the solid phase was dispersed in 10 mL solution at pH = 7.4 and pH = 5. The drug release process was checked at fixed time intervals (1 h, 3 h, 5 h, 8 h, 18 h, 24 h, and 48 h).

2nd procedure: after adsorption of 5-FU and pores blocking by β-CD, pH was kept at 7.4 The solution was checked every 2 h during 10 h period to verify that there is no drug release. Then, pH was adjusted to 5 and the drug release process was again checked at fixed time intervals (1 h, 3 h, 5 h, 8 h, 18 h, 24 h, and 48 h).

2.4. Characterization of porous solids and analytical techniques

Nitrogen sorption measurements were carried out using an ASAP 2010 Micromeritics apparatus at −196 °C. Prior to adsorption, samples (~80–100 mg) were outgassed at 120 °C during 12 h under the vacuum of 2.10^{-3} mbar. The specific surface area was determined with Brunauer, Emmet, and Teller (BET) method, the pore size distribution was calculated from the adsorption branch using the Barrett-Joyner-Halenda (BJH) method [41].

TEM micrographs were obtained using a JEOL 2000FX microscope. Samples were ground and afterward suspended in methanol. The suspension was added to a carbon grid and dried in air.

UV–Visible spectroscopy measurements in the liquid phase were performed on a Varian Cary 300 spectrometer in the 300–800 nm range.

Thermogravimetric (TGA) measurements were carried out with a TGA Q500 apparatus (TA Instruments) using air as a carrier gas. The samples (~5–20 mg) were treated up to 800 °C.

Small-angle X-Ray diffraction measurements were recorded on a Siemens D500R XRD diffractometer using Cu Kα radiation in the 0.5 − 3° 2θ range with a 0.04° step associated with a step time of 4 s.

2.5. The interaction of mesoporous silica SBA-15 and SBA-15_N-ANI_5-FU_β-CD with cancer cells

The human glioma cells U87 MG (Cells Lines Services, Germany) were used as a model of cancer cells for microscopy and cell viability study. The cell cultures were grown in the complete cell culture medium Dulbecco's modified Eagle medium (D-MEM, GlutaMAX™, Gibco-Invitrogen, Life Technologies Ltd., France) supplemented with 10% fetal bovine serum (FBS, biosera, France) in dark at 37 °C, 5% CO_2 and 80% humidified atmosphere.

2.5.1. The cytotoxicity of SBA-15 and SBA-15_N-ANI_5-FU_β-CD: MTT assay

The U87 MG cells were seeded into 96-well plates (10^4 cells/well) and 24 h after seeding the 5-FU, SBA and SBA-15_N-ANI_5-FU_β-CD aliquots (dissolved in the distilled water) were administered into the complete cell culture media. The cells were treated during 24 h with the 0.02 and 0.05 mg/mL of 5-FU, 0.6 and 1.5 mg/mL of SBA-15, and 0.8 and 2 mg/mL of SBA-15_N-ANI_5-FU_β-CD at pH = 7.3 and 6.3. The pH of cell culture media was adjusted with HCl (Sigma-Aldrich, Germany) 24 h before administration of the nanoparticles. After the treatment, the MTT (3-(4,5-dimethylthiazol-2-yl)-2,5-diphenyltetrazolium bromide, Sigma-Aldrich, Germany) assay was detected at 560 nm and 750 nm by 96-well plate absorption reader (GloMax®-Multi + Detection System with Instinct Software, Promega Corporation, USA). The ten μl of the yellow MTT reagent (5 mg/mL) dissolved in phosphate saline buffer solution (PBS, Sigma-Aldrich Germany) at pH = 7.4 were added to 100 μL of cell culture media per well. The cells were incubated with MTT in dark and 37 °C during 1 h. After the incubation, the medium was replaced with dimethyl sulfoxide (DMSO, Sigma-Aldrich, Germany) to dissolved purple formazan crystals. The results were performed in triplicates.

2.5.2. The cytotoxicity of SBA-15 and SBA-15_N-ANI_5-FU_β-CD: The mitochondria membrane potential dissipation

The U87 MG cells were seeded in Petri dishes (35 mm) and grown in the complete cell culture media at pH 7.3 and 6.3. The 1.5 mg/mL of SBA-15 and 2 mg/mL of SBA-15_N-ANI_5-FU_β-CD were administered to cells 24 h before observation. The mitochondria potential probe a MitoTracker™ Orange CMTM/Ros (MTO, 0.2 μM, ThermoFisher Scientific, USA) was administered to cells last 15 min of incubation with the nanoparticles. The cells were detached with the trypsin/ethylenediaminetetraacetic acid (Gibco-Invitrogen, Life Technologies Ltd., France), centrifuged at 1200 rpm/10 min and resuspended in 0.5 mL of PBS.

Alternatively, cells were harvested with the trypsin/EDTA, centrifuged and resuspended in the serum-free D-MEM. Subsequently, cells were incubated with 0.01 and 0.05 mg/mL of 5-FU, 0.3, 0.6 and 1.5 mg/mL of SBA-15, and 0.4, 0.8 and 2 mg/mL of SBA-15_N-ANI_5-FU_β-CD in the 100 μL of D-MEM during 1 h in dark, at pH = 7.3 and 37 °C. The mitochondria and lysosomes were stained 15 min before measurement with the MTO and the LysoTracker™ Green DND-26 (0.2 μM, ThermoFisher Scientific, USA).

The harvested cells were measured with the flow cytometer (MACSQuant® Analyzer, Miltenyi, Germany) in B1 (525/50 nm) and B3 (655–730 nm) channel at the excitation 488 nm.

2.5.3. The intracellular distribution and uptake of SBA-15 and SBA-15_N-ANI_5-FU_β-CD by U87 MG cells

The U87 MG cells were seeded in glass coverslip bottom Petri dishes (35 mm, No. 0, MatTek, USA) at the density of 10^4 cells per Petri dish. The white field and fluorescence images were recorded with the inverted LSM700 confocal microscope (Zeiss, Germany), equipped with a 20X Fluar (NA = 0.75, ∞, Zeiss, Germany) and a CCD camera (AxioCam HRm, Zeiss, Germany). The mitochondria were detected with the MTO. Thy lysosomes were stained with LysoTracker™ Green DND-

26 and the nuclei of the cells were contrasted with 10 μg/mL Hoechst 33,258 (Hoechst, 15 min, ThermoFisher Scientific, Slovakia). The fluorescence of mitochondria and lysosomes was stimulated by 488 nm and 555 nm cw solid-state lasers, and the emission was detected in the spectral range 490–540 nm and > 580 nm, respectively. The nuclei were visualized by 405 nm laser excitation and the emission was detected in the range 410–490 nm. The images were analyzed in Zen 2011 software (Zeiss, Germany) or ImageJ software (National Institutes of Health, USA). The aliquots of 5-FU, SBA and SBA-15_N-ANI_5-FU_β-CD were administered 24 h before observation with the microscope. The pH of cell culture media was adjusted with HCl (Sigma-Aldrich, Germany) 24 h before administration of the nanoparticles. The cells were grown in the complete cell culture media at pH = 7.3 and 6.3.

3. Results and discussion

There are different types of periodic mesoporous silicas, like MCM-41, MCM-48, SBA-16, SBA-12, SBA-15 which can be used as matrices in the design of DDSs. All of these we have tested in our previous studies as DDS [12–14,42,43]. For example, when we prepared materials, which release the drug using electromagnetic radiation as physical stimulus, we have used MCM-41 [43] or SBA-12 [12], since these materials have pore size around 3–4 nm, which is suitable for grafting of photoactive ligands and reversible formation/splitting of dimers by cycloaddition reaction. When using silica with larger pores, e.g. SBA-15, this cycloaddition reaction would be less favorable to regulate pore closing/opening. However, in the present study, we have used SBA-15 silica with larger pores. In materials like MCM-41, with narrower pores or SBA-16, with ink bottle pores, the grafting of bulky ligands, like N-ANI, would lead to pore blocking. In SBA-15 silica, the pore size is large enough to adapt both bulky amines as well as the drug. Moreover, SBA-15 material has large pore volume and possesses high stability.

For the silica modification and formation of the stalks on the surface, three different amines were grafted onto the mesoporous silica surface. Aliphatic amines namely propylamine (AP), tetraethylenepentamine (TEPA) and the aromatic amine propyl aniline (N-ANI) were used.

In the study, we have used 5-FU as a model drug. This drug is used in the clinical medicine for cancer treatment, however, at the present time, its efficiency is limited by many factors such as high rate of metabolism in the body, short biological half-life, non-uniform oral adsorption, and cytotoxicity. We expect, that its encapsulation in a host porous system presenting sustained drug release properties will potentially reduce the frequency of administration of the drug, reduce the adverse side effects and prolong its delivery time and elimination in the body [44].

3.1. Structure and porosity of SBA-15 and SBA15_N-ANI

The porosity of the starting SBA-15 material and its modified forms was studied using Transmission Electron Microscopy (TEM). TEM images (see Fig. 1a) shows a regular hexagonal array of unimodal channels perpendicular to the pore direction and parallel to the channels (Fig. 1b). The average pore size and the particle size determined from TEM images were 7 nm and 550 × 350 nm, respectively. After surface modification, 5-fluorouracil loading and β-CD capping the mesostructured, as evident by TEM, remained unchanged (Fig. 1c-f).

In addition to TEM, the periodicity of the samples was also studied using SAXS. Fig. 2 displays the XRD patterns of SBA-15 and SBA-15_N-ANI. For both samples, the XRD patterns are similar and show three resolved diffraction peaks that can be indexed with (1 0 0), (1 1 0), (2 0 0) reflections of the *p6mm* hexagonal structure [45].

Textural properties of the prepared mesoporous materials were further studied using N_2 adsorption/desorption measurements at 77 K. The N_2 adsorption/desorption isotherms of the SBA-15 and SBA-15_N-ANI are shown in Fig. 3.

Adsorption isotherms are characterized by an initial sharp uptake at a relative pressure below 0.05 followed by a more gradual uptake before a second sharp upswing in the curves between relative pressures of 0.6 and 0.7 depending on samples. A final plateau ends the adsorption branch. Such isotherms can be defined by the IUPAC as mixed type I and type IV isotherms, attributed to samples containing both microporosity and mesoporosity [46]. Furthermore, the adsorption isotherms exhibit well-defined H1 hysteresis loops that are typical for SBA-15 mesoporous silica. The presence of the H1 hysteresis loop confirms the open-ended hexagonal cylindrical pore geometry [47]. Hysteresis loops have sharp adsorption-desorption branches indicating a narrow pore size distribution in prepared mesoporous samples. The equivalent surface areas were calculated using the BET method. The values of the BET surface area can be taken only to estimation because of the presence of microporosity, so the term “equivalent” BET surface area is used. These BET values are given in Table 1. The size of the mesopores was estimated using the BJH method applied to the adsorption branch of the isotherms and the values obtained are also given in Table 1 with the ones of mesopore volumes [41].

As expected, the specific surface areas and total pore volumes decrease significantly upon functionalization of SBA-15 by N-ANI ($400\ m^2{\cdot}g^{-1}$, $0.46\ cm^3{\cdot}g^{-1}$) compared to the corresponding values for pure SBA-15 ($790\ m^2{\cdot}g^{-1}$, $0.57\ cm^3{\cdot}g^{-1}$). The functionalization also downshifts the capillary condensation step to lower pressures. The shift of the adsorption step to lower relative pressures reflected the ‘filling’ of the pores. It also decreases the pore size in the modified materials from the 7 nm (pure SBA-15) to 6 nm (SBA-15_N-ANI).

Thermogravimetric analysis (TGA) measurements were performed in order to estimate the amounts of the amine groups grafted on the silica surface (see Fig. 5). As solvents losses occur in the 25–150 °C range, all TGA curves were normalized at T = 150 °C to not take into account their presence. The original TGA curves are shown in Supplementary information Fig. S3. The TGA curve of calcined SBA-15 evidences that the sample is thermally stable and no significant mass loss was observed in all range measured. Above 500 °C, a small weight loss (3.6 wt%) was observed corresponding to the silanol groups condensation and dehydroxylation of the sample. The functionalized mesoporous silica SBA-15_N-ANI is thermally stable up to 200 °C. The mass loss step, observed above this temperature, corresponds to the thermal decomposition of amine N-ANI ligands present on the surface of SBA-15. The total mass loss in the temperature range 200–750 °C is close 16.6 wt%. The corresponding amount of the N-ANI molecules grafted on the surface of calcined silica was calculated from the mass differences observed for SBA-15 and SBA-15_N-ANI samples. Amount of N-ANI molecules grafted on the surface of calcined silica material was calculated to be $1.26\ mmol.g^{-1}$. This amount is similar to the one found in the literature using the same grafting procedure [48].

3.2. Loading of 5-fluorouracil

The adsorption isotherms of 5-FU both on SBA-15 and SBA15_N-ANI porous solids determined at 25 °C in water conditions are presented in Fig. 4 (left). For both solids, similar adsorption isotherms of Langmuir type were found. The shape of isotherms corresponds to an L-type one [49]. This type of adsorption isotherm is frequently found in the case of a homogeneous and narrow distribution of energetic adsorption sites. L-type isotherm can be plot by the mathematical expression:

$$q_{ads} = q_{max} \cdot \frac{K.\ C_{eq}}{1 + K.\ C_{eq}} \tag{2}$$

where q_{max} ($mol.g^{-1}$), K (M^{-1}) and C_{eq} (M) represent the maximum adsorbed amount, the apparent equilibrium constant and the 5-FU equilibrium concentration. Very good correlation coefficients, 0.997 for SBA-15 and 0.993 in the case of SBA-15_N-ANI samples, were found between L-type isotherm expression and experimental results. The fits

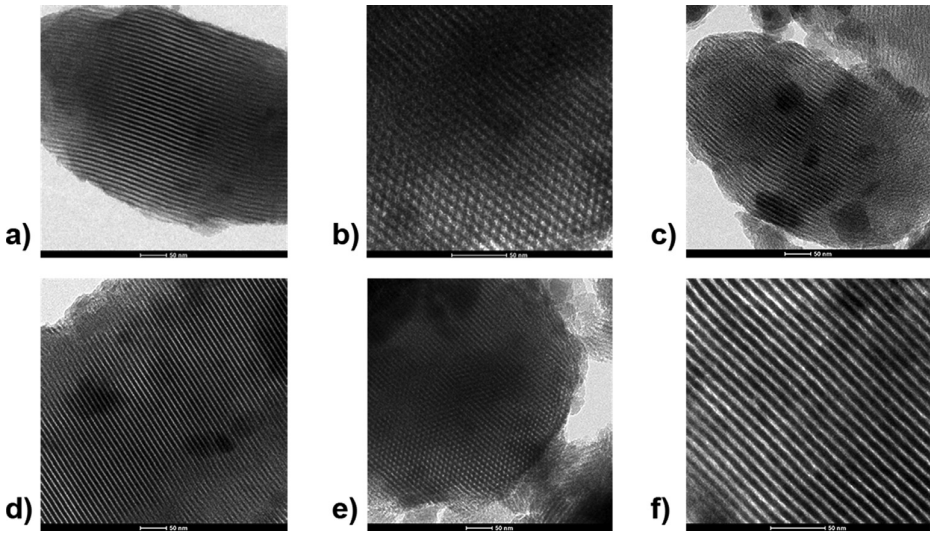

Fig. 1. TEM images of (a) and (b) SBA-15 after calcination and its modified forms (c) SBA-15_N-ANI, (d) SBA-15_N-ANI_5-FU, (e) and (f) SBA-15_N-ANI_5-FU_β-CD.

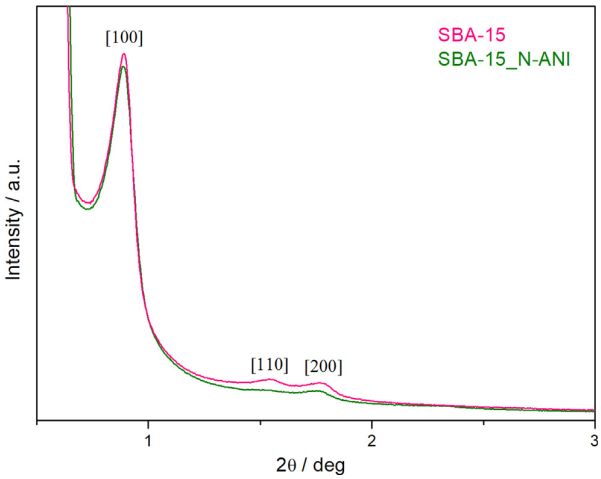

Fig. 2. Small-angle XRD diffractogram of the mesoporous silica SBA-15 and SBA-15_N-ANI.

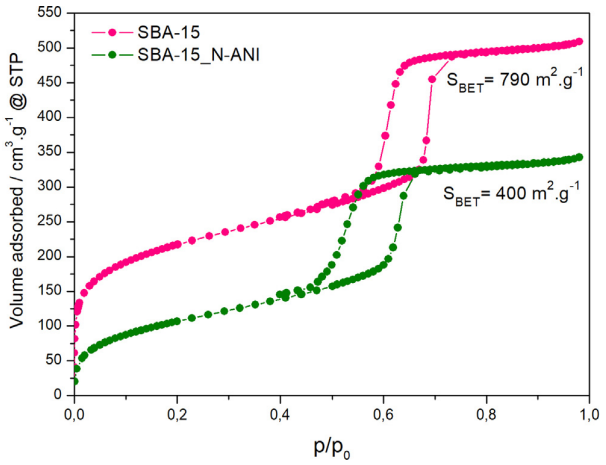

Fig. 3. Adsorption/desorption isotherms of the prepared samples SBA-15 and SBA-15_N-ANI.

Table 1
Surface area, mesopore size and mesopore volume of samples SBA-15 and SBA-15_N-ANI.

SAMPLE	S_{BET} [$m^2 \cdot g^{-1}$]	Mesopore volume [$cm^3 \cdot g^{-1}$]	Mesopore size [nm]
SBA-15	790	0.57 ± 0.3	7 ± 0.4
SBA-15_N-ANI	400	0.46 ± 0.3	6 ± 0.4

of the adsorption isotherms lead to maximum 5-FU adsorbed amounts of (12.8 ± 0.8) 0.10^{-4} $mol \cdot g^{-1}$ and (8.6 ± 1.8) 0.10^{-4} $mol \cdot g^{-1}$ corresponding to around 170 $mg.g^{-1}$ and 107 $mg \cdot g^{-1}$ for SBA-15 and SBA-15_N-ANI respectively. The affinity of 5-FU for each solid obtained by the fit appears weak from (29 ± 3) for SBA-15 to (22 ± 7) for SBA-15_N-ANI. These values are clearly evidenced considering the slope of adsorption isotherms at low concentrations. Thus, the main difference between the two solids concerns the maximum adsorbed amount and not especially the affinity, the former parameter is directly related to the surface area of solid. To illustrate this point, a direct calculation of the adsorbed amount corresponding to a 5-FU equilibrium concentration of $4.5.10^{-2}$ $mol \cdot L^{-1}$ leads to values of $7.3.10^{-4}$ $mol \cdot g^{-1}$ for SBA-15 versus $4.2.10^{-4}$ $mol \cdot g^{-1}$ for SBA-15_N-ANI. This diminution, close to 45%, is the same than the one observed between the surface areas calculated by BET for the two solids. The loading efficiency of 5-FU was 8.46% which represents 55 mg of 5-FU per 1 g of solid. Furthermore, the thermodynamic parameters determined from adsorption isotherms are very interesting. Indeed, high adsorbed amounts coupled with weak affinities should facilitate the release of a sufficient dose of 5-FU. In order to complete the adsorption study, calorimetric experiments were performed.

Obtained calorimetric results are very similar for both solids and confirm the interpretation of adsorption isotherms. Indeed, the plots of the integral enthalpies of displacement against the adsorbed amounts onto SBA-15 and SBA-15_N-ANI indicate a constant enthalpy of adsorption during the adsorption process. The associated values are close to (–3 ± 1) $kJ \cdot mol^{-1}$ and (–4 ± 1 $kJ \cdot mol^{-1}$) for SBA-15 and SBA-15_N-ANI respectively (Fig. 4 (right)). These weak values of adsorption enthalpies coupled with the absence of significative evolution along the surface coverage are characteristic of a narrow and homogenous energetic sites distribution. This set of parameters corresponds to a weak affinity during the physisorption of 5-FU on the two solids. The specific surface area limits the adsorbed amount and the presence of N-ANI

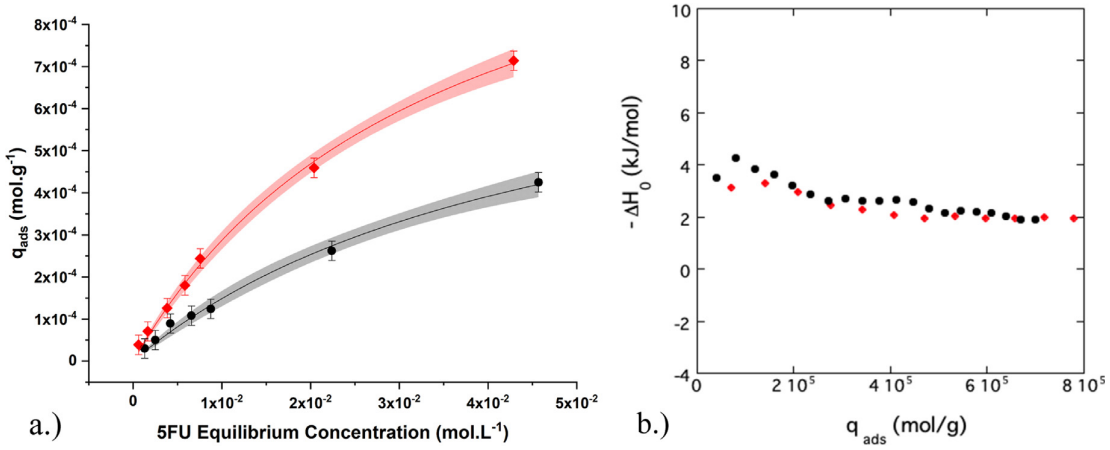

Fig. 4. (a.) Adsorption isotherms of 5-Fluorouracil onto SBA-15 and SBA-15-N-ANI. The line corresponds to the L type model and the shade bands around the fit represent the confidence interval of 95%. (b.) Corresponding enthalpograms. Diamonds and circles represent the SBA-15 and the SBA-15_N-ANI, respectively.

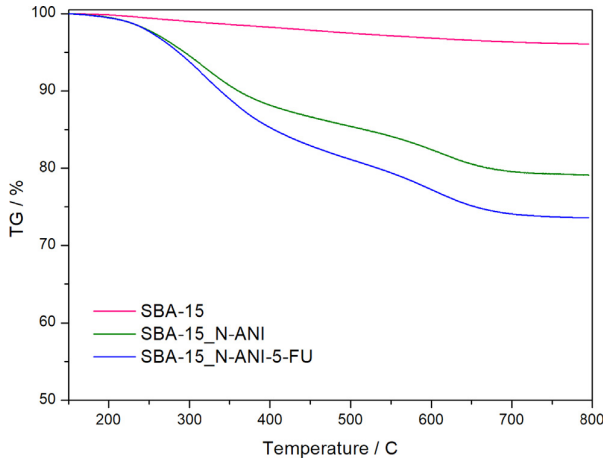

Fig. 5. TG curves of all prepared materials.

groups do not seem involved in the interaction.

The 5-FU loading was also studied using TGA measurements. First, the thermal behavior of the pure drug molecule was studied: it decomposes in one single step below 320 °C (Fig. S3, left in the Supplementary information) and in the range of 200–750 °C for the 5-FU loaded SBA-15_N-ANI_5-FU sample (Fig. 5, blue curve). The extended decomposition range for the 5-FU loaded sample is due to the interactions of a drug molecule with mesoporous channels and N-ANI ligands on the surface of silica. The trend of TGA curve of SBA-15_N-ANI_5-FU (Fig. 5, blue curve) is the same as the trend we observed for SBA-15_N-ANI sample (Fig. 5, green curve), but a total mass loss in the same temperature range is 22.46 wt%. The corresponding amount of the loaded 5-FU was calculated from the mass differences observed for SBA-15_N-ANI and SBA-15_N-ANI_5-FU samples. This difference represents 5.89 wt% that corresponds to 58,9 mg of 5-FU per 1 g of the carrier SBA-15_N-ANI_5-FU. This mass of loaded 5-FU is in good agreement with the one obtained from adsorption isotherms described above.

From the results obtained, it looks that the larger amount of the 5-FU was encapsulated in the pure, unmodified SBA-15 (92.63 $mg \cdot g^{-1}$, 0.712 $mmol \cdot g^{-1}$) compare to the modified silica SBA-15_N-ANI (55.3 $mg \cdot g^{-1}$, 0.425 $mmol \cdot g^{-1}$). However, these values do not reflect the ability of the material to adsorb the drug because they exhibit different specific surface areas. Taking into account this fact, the adsorbed amounts of the drug are 0.901 $mmol \cdot m^{-2}$ for SBA-15 and 1.0625 $mmol \cdot m^{-2}$ for SBA-15_N-ANI, thus in the same order of magnitude.

3.3. pH-sensitive release of 5-Fluorouracil

3.3.1. Description of the system containing β-cyclodextrin

The typical thermogram (in the air) of the studied β-CD is represented in Fig. S4 (right) in the Supplementary information. Weight loss found at 307 °C was related to the decomposition of β-CD structure due to the transition from solid to liquid phase and formation of a residue ("char"). At high temperatures > 350 °C complete oxidation (combustion) of the residue occurs (between 350 and 570 °C) with one step of weight loss [50]. Using the total mass loss for the sample SBA-15_N-ANI_5-FU_β-CD (Fig. S4 in the Supplementary information) the ratio of the N-ANI ligands on the external surface of silica and β-CDs capped is close to 1: 4.

The 5-FU loading and β-CD capping were also studied by adsorption/desorption of N_2 measurements at 77 K (see Fig. S5 in the Supplementary information). As expected, the specific surface areas and total volumes decrease upon 5-FU loading (285 $m^2 \cdot g^{-1}$, 0.33 $cm^3 \cdot g^{-1}$) and particles capping by β-CD (60 $m^2 \cdot g^{-1}$, 0.06 $cm^3 \cdot g^{-1}$) compared to the corresponding values for pure SBA-15_N-ANI (400 $m^2 \cdot g^{-1}$, 0.46 $cm^3 \cdot g^{-1}$). This decrease of around 80% demonstrates the very good efficiency of the use of β-CD molecules as nanovalves. The porous structure is almost not accessible after capping pores by β-CD molecules.

3.3.2. Zeta potential

Zeta (ζ) potential measurements were performed in aqueous suspensions at different pH values to determine the surface charge and stability of the prepared materials (see Fig. 6). The pure SBA-15 showed a negative ζ potential of about −78.8 mV due to the presence of terminal silanol groups on the surface of silica that was deprotonated at neutral pH, which is above the isoelectric point of silica. When pH decreases to 5 the ζ potential slightly changed to less negative values, in accordance with data obtained for other silica-based materials [51,52]. For the material SBA-15_N-ANI, the deprotonation of amines present on the surface occurs at pH 7.4, as reflected by the values of ζ potential with a negative surface charge −87.7 mV. Furthermore, a high zeta potential above 40 mV indicates that the grains of the samples do not agglomerate and are physically stable [53]. The change in pH to 5 led to an increase of ζ potential to positive values +5.7 mV (pK_a(N-ANI) = 5.04) [32], corresponding to the protonation on the N-aniline ligands. Obtained results indicated that material SBA-15_N-ANI, with protonation/deprotonation of amines on the surface, is promising for

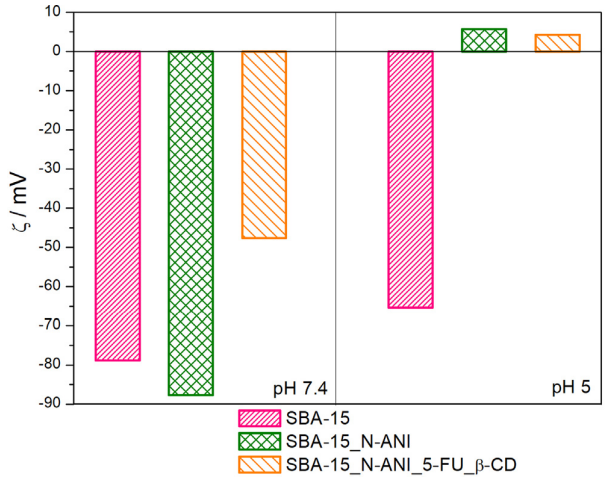

Fig. 6. Zeta potentials of prepared mesoporous materials in different pH media.

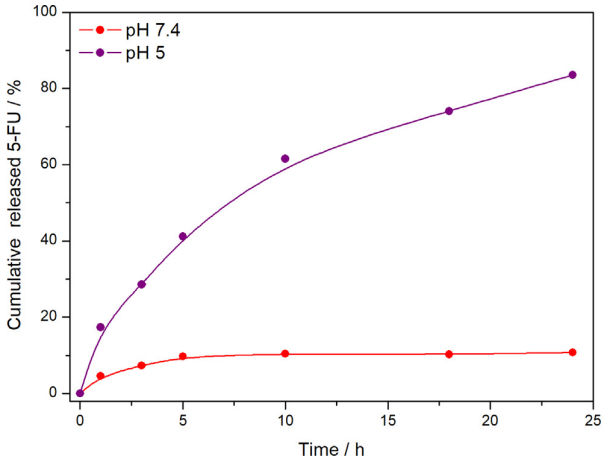

Fig. 7. The release profile of 5-FU from solid SBA-15_N-ANI_5-FU_β-CD in saline solution at two different pH (7.4, red curve and 5, purple curve).

use as a stalk in the designed pH-responsive DDS. After loading of SBA-15_N-ANI material with 5-FU and capping by β-CD, N-ANI ligands on the surface interact with cyclodextrin molecules, leading to the reduction of zeta potential to −47.6 mV at pH 7.4. At pH 5, when protonation of N-ANI molecules occurs, hydrogen bonds formed in supramolecular system amine-β-CD disappeared and effected zeta potential value to +4.27 mV, is similar to the sample SBA-15_N-ANI itself. The results of the zeta potential measurements confirm the mechanism of gate closing and opening through the formation of hydrogen bonds between the amine groups and β-CD driven by pH change.

3.3.3. *Drug release study*

Drug release studies were performed in solution, at two different pH values (~7.4 and ~5). The total loaded amount of 5-FU was established from the adsorption isotherm (Fig. 4) to be 55 mg (0.425 mmol·g^{-1}) per 1 g of solid SBA-15_N-ANI_5-FU, what was also confirmed by TGA measurements (Fig. 5). This amount was taken as 100% in the release studies and was used to calculate the percentage of the released amount in the respective time intervals. As it was mentioned above the release experiments were performed by two different procedures, in static and dynamic conditions.

3.3.3.1. Static conditions. The **1st procedure** was performed in order to check the efficiency of the couple β-CD/aromatic amines as 'gatekeepers' of mesoporous channels for the 5-FU drug. In this case, experiments were performed separately at two different pH, 7.4 and 5. The experimental results of drug release experiments are given in Fig. 7. As expected, there is a big difference between release profiles of 5-FU at pH = 7.4 and pH = 5. In the case of pH fixed at 7.4, a release of 10% of 5-FU in the initial 5 h was observed. This release could be explained by the fact that not all the porous channels were capped by β-CD molecules and the drug was released from these channels. No release of 5-FU was observed in the next 20 h that leads us to the conclusion that the couple β-CD/aromatic amine is efficient as a tight gatekeeper. When acidic conditions (pH = 5) were applied, a faster release rate of the drug was observed due to the change in the interaction between β-CD and aromatic amines groups. Decrease of pH caused that the groups of N-ANI on the surface of silica become protonated, resulting in a decreased binding affinity to the β-CD. The β-cyclodextrin caps are thus dispersed around from the stalks and pores are un-blocked leading to drug release. From the beginning to the end of the release process, the drug was released from the matrix gradually, when 41% of 5-FU was released in the first 5 h and in total, 86% of 5-FU was released within 24 h.

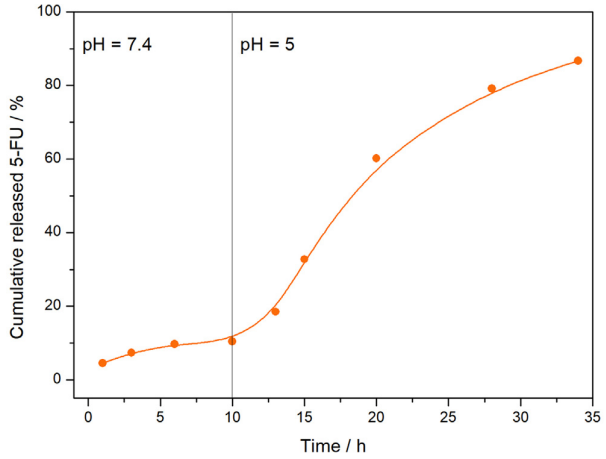

Fig. 8. The release profile of 5-FU from the solid SBA-15_N-ANI_5-FU_β-CD before and after adjusting pH to 5.

3.3.3.2. Dynamic conditions. The main purpose of the **2nd procedure** was to study the drug release behavior when the pH is changed from basic to acidic in the same release media. As shown in Fig. 8 and as expected, no additional release of 5-FU was observed at pH = 7.4 (compared with static conditions). After adjusting the pH to lower value (~pH 5), the release process started immediately. After changing pH, 86% of 5-FU was released gradually in 24 h.

The interaction between β-cyclodextrin molecules and aromatic amine groups was studied using microcalorimetry by decreasing the pH medium. With the decrease of pH, an exothermic signal is observed in the pH range (7.4 to 5). This signal is certainly related to the release in the liquid phase of β-cyclodextrin molecules. Nevertheless, the observed heat variation cannot be directly attributed to the internal energy change of a specific phenomenon (see Table 2).

3.3.4. *Kinetics of drug release*

The mechanism of 5-FU *in-vitro* release from SBA-15_N-ANI_5-FU_β-CD system was also studied from a kinetic point of view. In general, the release kinetics of drugs from ordered mesoporous materials mainly follows First order model or Higuchi one [54–57]. While the First Order model is general, the Higuchi one can be used for the description of drug release from spherical systems and various geometric porous matrices [58]. Equation of Higuchi model is reuniting the main factors that take part in the release of a drug, e.g.: diffusion of the drug in

Table 2
Summarization of the values obtained from the thermal analysis, N_2 adsorption/desorption measurements and solid/liquid adsorption measurements.

SAMPLE	N-ANI grafted, n [mmol·g^{-1}]	S_{BET} [m^2·g^{-1}]	5-FU, n_{ADS} [mmol·g^{-1}]	5-FU, n_{ADS} [mmol·m^{-2}]	5-FU, m_{ADS} [mg·g^{-1}]	5-FU, m_{ADS} [mg·m^{-2}]
SBA-15		790	0.712	0.901	92.63	0.117
SBA-15_N-ANI	1.26	400	0.425	1.0625	55.3	0.138

Table 3
Coefficient of determination values for the two drug release kinetics models of SBA-15_N-ANI_5-FU_β-CD.

First order		Higuchi model	
r^2	K_1 [h^{-1}]	r^2	K_h [h$^{-0,5}$]
0.9913	0.06863	0.9914	17.486

dissolvent, the tortuosity factor of the system, the porosity of the matrix, total amount of drug in the matrix and the solubility of the drug in the solvent used [59]. The limitation linked to drug solubility that is one basis of the Higuchi model is not validated in our case. Nevertheless, as shown in Table 3, it was found that the *in vitro* release of 5-FU from SBA-15_N-ANI_5-FU_β-CD at pH 5 could be explained by both Higuchi's and First order models, as the plots showed the highest linearity with the coefficient of determination (COD) equal to 0.9913 and 0.9914 respectively. The values of kinetic constants were $K_1 = 0.0663\,h^{-1}$ for First order model and $K_H = 17.486\,h^{-0,5}$ for Higuchi model. The quasi-identical values of COD can be explained considering that the drug kinetics release from the porous system is not affected by the oversaturation step inherent from the Higuchi model.

3.4. The cytotoxicity of SBA-15 and SBA-15_N-ANI_5-FU_β-CD systems in U87 MG cells

The human glioma U87 MG cells were demonstrated to represent the glycolytic type of the cancer cells model [60]. Since certain tissue and the tumors have more acidic pH than the normal tissue [61], we have investigated the 5-FU, SBA-15 and SBA-15_N-ANI_5-FU_β-CD at physiological (pH = 7.3) and acidic (pH = 6.3) pH of the cell culture media.

The morphology of U87 MG cells at both pH in the presence of 0.05 mg/mL of 5-FU, 1.5 mg/mL of SBA-15 and 2 mg/mL of SBA-15_N-ANI_5-FU_β-CD is presented in Fig. 9a. The cells were incubated with the systems 24 h and the significant changes in the morphology of the cells were not found (see white arrows that identify the cells). The SBA-15 and SBA-15_N-ANI_5-FU_β-CD systems were observed in the dark clouds localized in the extracellular media close to the cells. It can be seen that the localization of these clouds is not homogeneous.

The viability of cells in the presence of 0.05 mg/mL of 5-FU, 1.5 mg/mL of SBA-15 and 2 mg/mL of SBA-15_N-ANI_5-FU_β-CD at pH = 7.3 and 6.3 was assessed with MTT assay (Fig. 9b). The drop of the extracellular pH caused inhibition of the cell proliferation in comparison with the cells at pH = 7.3. The 24 h treatment with 5-FU significantly decreased the proliferation. However, more than 80% of the cells were still active. This finding is in the agreement with previously published studies [62,63]. In those studies, the cytotoxic effect of 5-FU was observed at a concentration above 0.5 mg/mL but 48 h after 5-FU administration.

In the present study, the formation of formazan in the mitochondria of U87 MG cells was significantly inhibited in the presence of SBA-15 and SBA-15_N-ANI_5-FU_β-CD (Fig. 9b). Regarding the cell morphology detected by microscopy, these observations were unexpected. When we compare the results from microscopy images and MTT-assay it is evident that the morphology of the cells in the presence of SBA-15 and SBA-15_N-ANI_5-FU_β-CD did not change compared to the morphology of the controlled cells (Fig. 9a, right). We expected that results of the MTT-assay would also be similar to the control as it was with microscopy results. However, MTT-assay has shown that formation of formazan in the cells was significantly inhibited in the presence of SBA-15 and SBA-15_N-ANI_5-FU_β-CD (Fig. 9b).

In Hu and Zhao works [62,63], the 5-FU application increased the oxidative stress level in the cancer cells and resulted in the mitochondria membrane potential ($\Delta\Psi_m$) dissipation in further. The mitochondrial probes, especially MTO, can indicate oxidative stress and $\Delta\Psi_m$ in living cells [60,64]. The MTO fluorescence intensity in U87 MG cells detected by flow cytometry and fluorescence microscopy is demonstrated in Fig. 9c. While SBA-15 system slightly decreased the MTO fluorescence, the SBA-15_N-ANI_5-FU_β-CD system completely dissipated the $\Delta\Psi_m$. The mitochondrial localization of MTO was observed in the control and SBA-15 treated cells. No fluorescence was detected in the SBA-15_N-ANI_5-FU_β-CD treated cells. The similar results were observed at pH = 7.3 and 6.3. It suggests that the extracellular pH did not significantly influence the cell response to treatments.

The U87 MG cells express a higher number of receptors, which facilitate the endocytotic type of drugs transport [65]. It was demonstrated that in a relatively short time (within 1 h), the transport system can pass the membrane *via* endocytosis and subsequently localize in lysosomes of cancer cells [66]. The lysosomes of cells are the cellular compartments with acidic pH (pH = 5.5) [61]. As it was mentioned above, the SBA-15_N-ANI_5-FU_β-CD system is pH sensitive and 5-FU should be released from the system at pH = 5.5. The 5-FU is not fluorescent. For this reason, the indirect method was used to identify the release of 5-FU from the SBA-15_N-ANI_5-FU_β-CD.

The representative confocal fluorescence images of U87 MG cells 24 h treated with 5-FU, SBA-15, and SBA-15_N-ANI_5-FU_β-CD system are depicted in Fig. 10a. The cells were stained with MTO to visualized the mitochondria and LysoTracker™ Green to identify the lysosomal compartments. The nuclei of the cells were contrasted with Hoechst. The control group is represented with tubular mitochondria and globular lysosomes. The application of 0.02 mg/mL of 5-FU did not induce significant modifications. However, the application of 0.6 mg/mL of SBA-15 amplified fluorescence of LysoTracker™ Green. The tubular mitochondria were observed in the SBA-15 treated cells. It should be noted that the clouds of SBA-15 system in the extracellular area entrapped the number of fluorescent probes and significantly reduced Hoechst staining of nuclei. This effect was amplified in the SBA-15_N-ANI_5-FU_β-CD treated cells. The blue (Hoechst) fluorescence was mostly attributed to the SBA-15_N-ANI_5-FU_β-CD system localization (Fig. 10a). The MTO fluorescence completely disappeared in these cells. The swollen lysosomes can be identified from the images of LysoTracker™ fluorescence.

The cancer cells became highly adaptive to intracellular oxidative stress and revealed the way how to rescue and survive [60,67]. Recently, it was shown that the nanoceria applied to the U87 MG cells locally increased the oxidative stress level in the perinuclear area without affection of the cell proliferation [68]. One can expect the same behavior in cells treated with SBA-1. The MTT-assay, performed in the same cell as detected in Fig. 10a demonstrates a significant reduction of formazan production in SBA-15 and SBA-15_N-ANI_5-FU_β-CD treated cells (Fig. 10b). The almost 50% decrease observed could be the result of $\Delta\Psi_m$ dissipation, lysosomal destabilization, and induction of mitochondria-mediated apoptosis.

The correlation between MTO and LysoTracker™ Green fluorescence was measured by flow cytometry. The characteristic shift into

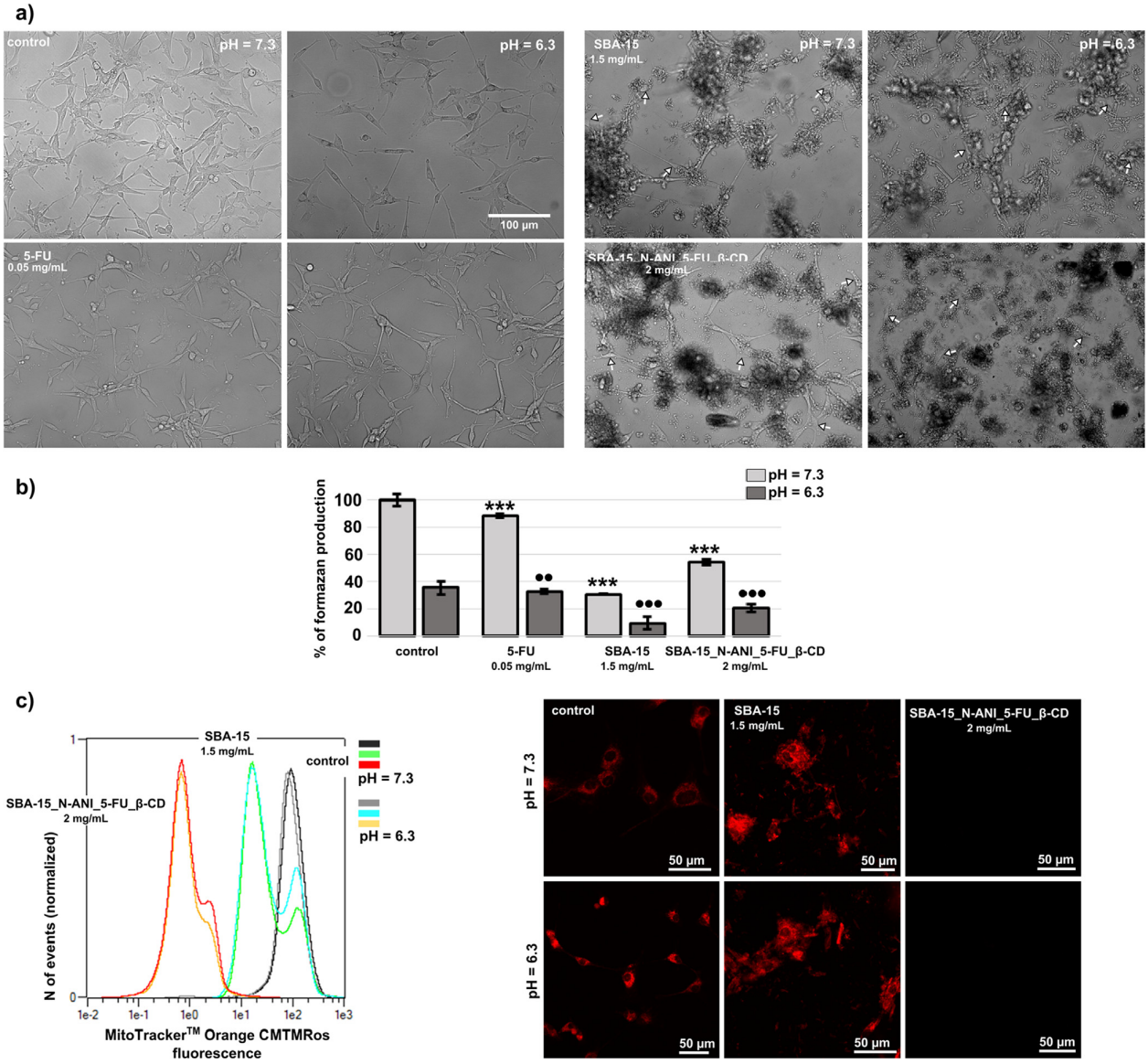

Fig. 9. The representative a) white-field images of U87 MG cells detected 24 h after application of 0.05 mg/mL 5-FU, 1.5 mg/mL SBA-15 and 2 mg/mL SBA-15_N-ANI_5-FU_β-CD at pH = 7.3 and 6.3 (the white arrows highlighted the cells). The MTT-assay b) was assessed in the cells at the same conditions as in a). The level of significance was calculated from the controls at pH = 7.3 (***$p < 0.001$) and pH = 6.3 (••$p < 0.01$ and •••$p < 0.001$). The mitochondria membrane potential c) was estimated with MTO staining by flow cytometry (left) and confocal fluorescence microscopy (right) at the same conditions as in a).

upper right quadrant was observed in the non-treated controlled cells labeled with the probes (Fig. 10c). This character maintained in the cells 1 h treated with 5-FU (0.01 and 0.05 mg/mL) and SBA-15 (0.3 and 0.6 mg/mL). The reduction of MTO fluorescence was found in the 50% of cells treated with 1.5 mg/mL of SBA-15. Lysosomal integrity has persevered. In contrast to SBA-15, the SBA-15_N-ANI_5-FU_β-CD system triggered dissipation of $\Delta\Psi_m$ and destabilization of lysosomes. The 79.68% of cells were detected in lower left quadrant (MTO negative and LysoTracker™ green negative) at 0.4 mg/mL concentration and 96.26% was observed at 2 mg/mL of the SBA-15_N-ANI_5-FU_β-CD.

These results demonstrated that the 5-FU did not induce cell death at the studied concentration and during 24 h. Furthermore, SBA-15 application to cells slightly decrease mitochondria membrane potential but SBA-15 adsorbed the certain number of applied fluorescent probe's molecules. Due to this effect, it could be assumed that the MTT was similarly entrapped into SBA-15 during MTT-assay, and subsequently resulted in a reduction of formazan production. The mitochondria dysfunction and SBA-15 absorption properties could be the reason for reduced formazan production, which was observed in the present study. For this reason, the direct estimation of the cell viability (MTT-assay) should be supplemented with indirect approaches ($\Delta\Psi_m$ and destabilization of lysosomes). These indirect approaches confirmed the cytotoxic effect of the SBA-15_N-ANI_5-FU_β-CD. Regarding to the total loading concentration of 5-FU, appropriate concentration of free 5-FU represents 0.018 mg/mL in 0.4 mg/mL SBA-15_N-ANI_5-FU_β-CD. As it was reported, this concentration of 5-FU was not cytotoxic if applied into cell culture media, neither after 48 h [62]. However, when it was delivered into the cells by SBA-15_N-ANI_5-FU_β-CD it possessed significant cytotoxic effects. The degradation of lysosomes was probably induced with 5-FU released from SBA-15_N-ANI_5-FU_β-CD within the lysosomes at pH = 5.5. The presence of SBA-15 within the cell could be suggested from the elevated levels of oxidative stress, which partially

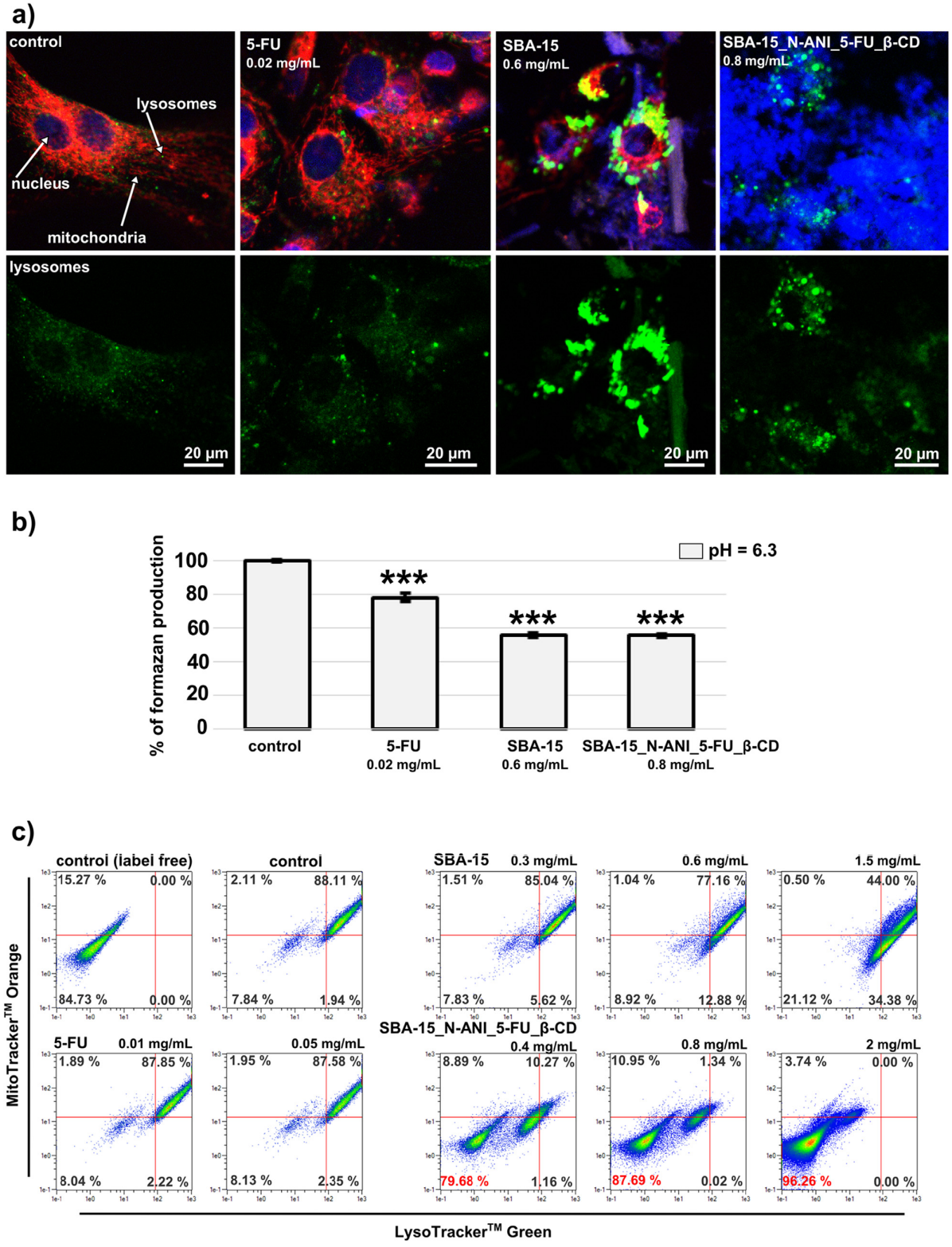

Fig. 10. The representative a) confocal fluorescence images of U87 MG cells detected 24 h after application of 0.02 mg/mL 5-FU, 0.6 mg/mL SBA-15 and 0.8 mg/mL SBA-15_N-ANI_5-FU_β-CD at pH 6.3. Mitochondria were visualized with MTO, the lysosomes with LysoTracker™ Green and nuclei were contrasted with Hoechst. The fluorescent images of lysosomes are depicted below the overlapped images. The MTT-assay b) was assessed in the cells at the same conditions as in a). The level of significance was calculated from the controls (***$p < 0.001$). The correlations of MTO and LysoTracker™ Green fluorescence c) were estimated by flow cytometry in cells 1 h treated with the 5-FU, SBA-15 and SBA-15_N-ANI_5-FU_β-CD at pH 7.3. The correlation plot was divided into four quadrants. The upper right quadrant represents the control cells positive for MTO and LysoTracker™ Green. The lower left quadrant characterizes the dissipation of the $\Delta\Psi_m$ and destabilization of lysosomes. The number of cells is identified by the color-code (blue – minimum, red – maximum).

caused the dissipation of $\Delta\Psi_m$. The SBA-15_N-ANI_5-FU_β-CD systems seems to be more effective in anti-cancer treatment than sole 5-FU.

4. Conclusions

A system based on mesoporous silica material was studied as a potential pH-sensitive drug delivery system for the antineoplastic agent 5-fluorouracil (5-FU). This system is composed of SBA-15-type porous structure (hexagonal) functionalized with aromatic primary amines (N-ANI) and β-cyclodextrin molecules (β-CD) that are used as nanovalves.

Starting from the synthesis and characterization of SBA-15 material, the successful functionalization of N-ANI groups was evidenced using thermogravimetric measurements ($n_{grafted} = 1.26$ mmol/g). Textural properties of functionalized samples were investigated using small angle XRD, TEM, and nitrogen sorption measurements that allow us to conclude that even if a decrease was observed in terms of specific surface area (−50%) and porous volume (−25%), the whole porous structure was preserved and available for drug molecules.

Then, the loading of the drug 5-FU in pure SBA-15 and SBA-15_N-ANI was studied from a thermodynamic point of view *via* the construction of adsorption isotherms and calorimetric measurements. For both solids, adsorption isotherms are of Langmuir type. The affinity of 5-FU molecules (linked to the slope of isotherms at low concentrations) towards both solids is weak. Calorimetric measurements evidenced a weak constant enthalpies of adsorption for both solids ($\Delta H = -3/-4$ kJ/mol). Finally, the only difference observed between both solids lies in the maximum adsorbed amounts of 5-FU determined both experimentally ($7.3 \cdot 10^{-4}$ mol/g vs $4.2 \cdot 10^{-4}$ mol/g); this difference is linked to the difference in specific surface area. The maximum loading of 5-FU determined from both the adsorption isotherm and thermogravimetric measurements for the N-ANI functionalized porous material was 55 mg/g.

The pH-sensitive release of 5-FU from SBA-15_N-ANI solid, using β-CD molecules as nanovalves, was finally investigated in static and dynamic conditions: it was shown that there was almost no release of 5-FU at pH = 7.4 whereas more than 80% of adsorbed 5-FU was progressively released at pH = 5. The modeling of the 5-FU release was successfully done using both first order and Higuchi models. The cytotoxicity tests were performed using human glioma U87 MG cells. The results demonstrated that the 5-FU did not induce cell death at the studied concentration if applied into cell culture media. However, when it was delivered into the cells by SBA-15_N-ANI_5-FU_β-CD it possessed significant cytotoxic effects.

Acknowledgments

This work was supported by the Slovak Research and the Development Agency under the contracts APVV-15-0520 and APVV-15-0485 and national bilateral grant APVV-SK-FR-2017-0011. E.B. thanks to the financial support from VVGS-PG-2017-677 grant. E.B. also thanks to the French Government for the financial support linked to the implementation of a joint French-Slovak doctorate. The authors thank the Ministry of Education, Science, Research and Sport of the Slovak Republic and the Accreditation Commission for the financial support of the TRIANGEL team in the frame of the scheme “Top Research Teams in Slovakia”.

References

[1] J. Lu, M. Liong, J.I. Zink, F. Tamanoi, Mesoporous silica nanoparticles as a delivery system for hydrophobic anticancer drugs, Small 3 (2007) 1341–1346, https://doi.org/10.1002/smll.200700005.

[2] T.P. Lodise, J. Graves, A. Evans, E. Graffunder, M. Helmecke, B.M. Lomaestro, K. Stellrecht, Relationship between vancomycin MIC and failure among patients with methicillin-resistant staphylococcus aureus bacteremia treated with vancomycin, Antimicrob. Agents Chemother. 52 (2008) 3315–3320, https://doi.org/10.1128/AAC.00113-08.

[3] K.K. Jain, ed., Drug Delivery Systems, Humana Press, 2008. //www.springer.com/us/book/9781588298911 (accessed September 4, 2018).

[4] T.M. Allen, P.R. Cullis, Drug delivery systems: entering the mainstream, Science 303 (2004) 1818–1822, https://doi.org/10.1126/science.1095833.

[5] J. Zhou, M. Wang, H. Ying, D. Su, H. Zhang, G. Lu, J. Chen, Extracellular matrix component shelled nanoparticles as dual enzyme-responsive drug delivery vehicles for cancer therapy, ACS Biomater. Sci. Eng. 4 (2018) 2404–2411, https://doi.org/10.1021/acsbiomaterials.8b00327.

[6] M. Zhang, F. Wu, W. Wang, J. Shen, N. Zhou, C. Wu, Multifunctional nanocomposites for targeted, photothermal, and chemotherapy, Chem. Mater. (2018), https://doi.org/10.1021/acs.chemmater.8b00934.

[7] L. Zhang, Y. Li, J.C. Yu, Chemical modification of inorganic nanostructures for targeted and controlled drug delivery in cancer treatment, J. Mater. Chem. B. 2 (2014) 452–470, https://doi.org/10.1039/C3TB21196G.

[8] S. Carrasco, E. Benito-Peña, F. Navarro-Villoslada, J. Langer, M.N. Sanz-Ortiz, J. Reguera, L.M. Liz-Marzán, M.C. Moreno-Bondi, Multibranched gold-mesoporous silica nanoparticles coated with a molecularly imprinted polymer for label-free antibiotic surface-enhanced raman scattering analysis, Chem. Mater. 28 (2016) 7947–7954, https://doi.org/10.1021/acs.chemmater.6b03613.

[9] A.L. Doadrio, J.C. Doadrio, J.M. Sánchez-Montero, A.J. Salinas, M. Vallet-Regí, A rational explanation of the vancomycin release from SBA-15 and its derivative by molecular modelling, Micropor. Mesopor. Mater. 132 (2010) 559–566, https://doi.org/10.1016/j.micromeso.2010.04.010.

[10] M. Moritz, M. Geszke-Moritz, Mesoporous silica materials with different structures as the carriers for antimicrobial agent. Modeling of chlorhexidine adsorption and release, Appl. Surf. Sci. 356 (2015) 1327–1340, https://doi.org/10.1016/j.apsusc.2015.08.138.

[11] E. Beňová, V. Zeleňák, D. Halamová, Miroslav Almáši, Veronika Petrul'ová, M. Psotka, A. Zeleňáková, M. Bačkor, V. Hornebecq, A drug delivery system based on switchable photo-controlled p-coumaric acid derivatives anchored on mesoporous silica, J. Mater. Chem. B. 5 (2017) 817–825, https://doi.org/10.1039/C6TB02040B.

[12] V. Zeleňák, E. Beňová, M. Almáši, D. Halamová, V. Hornebecq, V. Hronský, Photoswitchable nanoporous silica supports for controlled drug delivery, New J. Chem. 42 (2018) 13263–13271, https://doi.org/10.1039/C8NJ00267C.

[13] V. Zeleňák, D. Halamová, M. Almáši, L. Žid, A. Zeleňáková, O. Kapusta, Ordered cubic nanoporous silica support MCM-48 for delivery of poorly soluble drug indomethacin, Appl. Surf. Sci. 443 (2018) 525–534, https://doi.org/10.1016/j.apsusc.2018.02.260.

[14] D. Halamová, M. Badaničová, V. Zeleňák, T. Gondová, U. Vainio, Naproxen drug delivery using periodic mesoporous silica SBA-15, Appl. Surf. Sci. 256 (2010) 6489–6494, https://doi.org/10.1016/j.apsusc.2010.04.044.

[15] Y. Zhang, J. Wang, X. Bai, T. Jiang, Q. Zhang, S. Wang, Mesoporous silica nanoparticles for increasing the oral bioavailability and permeation of poorly water soluble drugs, Mol. Pharm. 9 (2012) 505–513, https://doi.org/10.1021/mp200287c.

[16] R. Mellaerts, R. Mols, J.A.G. Jammaer, C.A. Aerts, P. Annaert, J. Van Humbeeck, G. Van den Mooter, P. Augustijns, J.A. Martens, Increasing the oral bioavailability of the poorly water soluble drug itraconazole with ordered mesoporous silica, Eur. J. Pharm. Biopharm. Off. J. Arbeitsgemeinschaft Pharm. Verfahrenstechnik EV. 69 (2008) 223–230, https://doi.org/10.1016/j.ejpb.2007.11.006.

[17] A. Gulzar, S. Gai, P. Yang, C. Li, M.B. Ansari, J. Lin, Stimuli responsive drug delivery application of polymer and silica in biomedicine, J. Mater. Chem. B. 3 (2015) 8599–8622, https://doi.org/10.1039/C5TB00757G.

[18] T. Zhao, L. Chen, Q. Li, X. Li, Near-infrared light triggered drug release from mesoporous silica nanoparticles, J. Mater. Chem. B. 6 (2018) 7112–7121, https://doi.org/10.1039/C8TB01548A.

[19] Y. Wang, Y. Cui, J. Huang, D. Di, Y. Dong, X. Zhang, Q. Zhao, N. Han, Y. Gao, T. Jiang, S. Wang, Redox and pH dual-responsive mesoporous silica nanoparticles for site-specific drug delivery, Appl. Surf. Sci. 356 (2015) 1282–1288, https://doi.org/10.1016/j.apsusc.2015.07.151.

[20] P. Nadrah, F. Porta, O. Planinšek, A. Kros, M. Gaberšček, Poly(propylene imine) dendrimer caps on mesoporous silica nanoparticles for redox-responsive release: smaller is better, Phys. Chem. Chem. Phys. 15 (2013) 10740–10748, https://doi.org/10.1039/C3CP44614J.

[21] S.H. van Rijt, D.A. Bölükbas, C. Argyo, S. Datz, M. Lindner, O. Eickelberg, M. Königshoff, T. Bein, S. Meiners, Protease-mediated release of chemotherapeutics from mesoporous silica nanoparticles to ex vivo human and mouse lung tumors, ACS Nano. 9 (2015) 2377–2389, https://doi.org/10.1021/nn5070343.

[22] Y. Yang, J. Wan, Y. Niu, Z. Gu, J. Zhang, M. Yu, C. Yu, Structure-dependent and glutathione-responsive biodegradable dendritic mesoporous organosilica nanoparticles for safe protein delivery, Chem. Mater. 28 (2016) 9008–9016, https://doi.org/10.1021/acs.chemmater.6b03896.

[23] Q. Yang, S. Wang, P. Fan, L. Wang, Y. Di, K. Lin, F.-S. Xiao, pH-responsive carrier system based on carboxylic acid modified mesoporous silica and polyelectrolyte for drug delivery, Chem. Mater. 17 (2005) 5999–6003, https://doi.org/10.1021/cm051198v.

[24] C. Gao, H. Zheng, L. Xing, M. Shu, S. Che, Designable coordination bonding in mesopores as a pH-responsive release system, Chem. Mater. 22 (2010) 5437–5444, https://doi.org/10.1021/cm100667u.

[25] L. Xing, H. Zheng, Y. Cao, S. Che, Coordination polymer coated mesoporous silica nanoparticles for ph-responsive drug release, Adv. Mater. 24 (2012) 6433–6437, https://doi.org/10.1002/adma.201201742.

[26] C.-H. Lee, S.-H. Cheng, I.-P. Huang, J.S. Souris, C.-S. Yang, C.-Y. Mou, L.-W. Lo, Intracellular pH-responsive mesoporous silica nanoparticles for the controlled release of anticancer chemotherapeutics, Angew. Chem. Int. Ed. 49 (2010) 8214–8219, https://doi.org/10.1002/anie.201002639.

[27] J. Fan, S. Wang, W. Sun, S. Guo, Y. Kang, J. Du, X. Peng, Anticancer drug delivery systems based on inorganic nanocarriers with fluorescent tracers, AIChE J. 64 (2018) 835–859, https://doi.org/10.1002/aic.15976.

[28] H. Li, L.-L. Tan, P. Jia, Q.-L. Li, Y.-L. Sun, J. Zhang, Y.-Q. Ning, J. Yu, Y.-W. Yang, Near-infrared light-responsive supramolecular nanovalve based on mesoporous silica-coated gold nanorods, Chem. Sci. 5 (2014) 2804–2808, https://doi.org/10.1039/C4SC00198B.

[29] S.U.N. Yu-Long, Y. Ying-Wei, W.U. Wei, Z.S. Xiao-An, Supramolecular nanovalve systems based on macrocyclic synthetic receptors, Chem. J. Chin. Univ. 33 (2012) 1635–1642, https://doi.org/10.3969/j.issn.0251-0790.2012.08.001.

[30] A.E. Kaziem, Y. Gao, Y. Zhang, X. Qin, Y. Xiao, Y. Zhang, H. You, J. Li, S. He, α-Amylase triggered carriers based on cyclodextrin anchored hollow mesoporous silica for enhancing insecticidal activity of avermectin against Plutella xylostella, J. Hazard. Mater. 359 (2018) 213–221, https://doi.org/10.1016/j.jhazmat.2018.07.059.

[31] S. Angelos, Y.-W. Yang, K. Patel, J.F. Stoddart, J.I. Zink, pH-responsive supramolecular nanovalves based on cucurbit[6]uril pseudorotaxanes, Angew. Chem. Int. Ed. 47 (2008) 2222–2226, https://doi.org/10.1002/anie.200705211.

[32] H. Meng, M. Xue, T. Xia, Y.-L. Zhao, F. Tamanoi, J.F. Stoddart, J.I. Zink, A.E. Nel, Autonomous in vitro anticancer drug release from mesoporous silica nanoparticles by ph-sensitive nanovalves, J. Am. Chem. Soc. 132 (2010) 12690–12697, https://doi.org/10.1021/ja104501a.

[33] L. Bai, Q. Zhao, J. Wang, Y. Gao, Z. Sha, D. Di, N. Han, Y. Wang, J. Zhang, S. Wang, Mechanism study on pH-responsive cyclodextrin capped mesoporous silica: effect of different stalk densities and the type of cyclodextrin, Nanotechnology 26 (2015) 165704, , https://doi.org/10.1088/0957-4484/26/16/165704.

[34] A. Mathew, S. Parambadath, S.S. Park, C.-S. Ha, Hydrophobically modified spherical MCM-41 as nanovalve system for controlled drug delivery, Micropor. Mesopor. Mater. 200 (2014) 124–131, https://doi.org/10.1016/j.micromeso.2014.08.033.

[35] X. Zhu, C.-Q. Wang, pH and redox-operated nanovalve for size-selective cargo delivery on hollow mesoporous silica spheres, J. Colloid Interface Sci. 480 (2016) 39–48, https://doi.org/10.1016/j.jcis.2016.06.043.

[36] D.B.G. Williams, M. Lawton, Drying of organic solvents: quantitative evaluation of the efficiency of several desiccants, J. Org. Chem. 75 (2010) 8351–8354, https://doi.org/10.1021/jo101589h.

[37] D. Zhao, Q. Huo, J. Feng, B.F. Chmelka, G.D. Stucky, Nonionic triblock and star diblock copolymer and oligomeric surfactant syntheses of highly ordered, hydrothermally stable, mesoporous silica structures, J. Am. Chem. Soc. 120 (1998) 6024–6036, https://doi.org/10.1021/ja974025i.

[38] Y.-L. Fan, B.-Y. Fan, Q. Li, H.-X. Di, X.-Y. Meng, N. Ling, Preparation of 5-fluorouracil-loaded nanoparticles and study of interaction with gastric cancer cells, Asian Pac. J. Cancer Prev. 15 (2014) 7611–7615, https://doi.org/10.7314/APJCP.2014.15.18.7611.

[39] D. Kala, Jijo Thomas, Deepa V. Nair, Effect of pH on aminofunctionalized mesoporous silica nanoparticles loaded with 5-fluorouracil and its optimization, World Pharm. Pharm. Sci. 7 (2018) 1400–1419.

[40] S. Egodawatte, S. Dominguez, S.C. Larsen, Solvent effects in the development of a drug delivery system for 5-fluorouracil using magnetic mesoporous silica nanoparticles, Micropor. Mesopor. Mater. 237 (2017) 108–116, https://doi.org/10.1016/j.micromeso.2016.09.024.

[41] Adsorption by Powders and Porous Solids - 2nd Edition, (n.d.). https://www.elsevier.com/books/adsorption-by-powders-and-porous-solids/rouquerol/978-0-08-097035-6 (accessed November 23, 2018).

[42] V. Zeleňák, D. Halamová, A. Zeleňáková, V. Girman, Periodic 3D nanoporous silica modified by amine or SPION nanoparticles as NSAID delivery system, J. Porous Mater. 23 (2016) 1633–1645, https://doi.org/10.1007/s10934-016-0224-x.

[43] E. Beňová, V. Zeleňák, D. Halamová, M. Almáši, V. Petrul'ová, M. Psotka, A. Zeleňáková, M. Bačkor, V. Hornebecq, A drug delivery system based on switchable photo-controlled p-coumaric acid derivatives anchored on mesoporous silica, J. Mater. Chem. B. 5 (2017) 817–825, https://doi.org/10.1039/C6TB02040B.

[44] N.S. Rejinold, K.P. Chennazhi, S.V. Nair, H. Tamura, R. Jayakumar, Biodegradable and thermo-sensitive chitosan-g-poly(N-vinylcaprolactam) nanoparticles as a 5-fluorouracil carrier, Carbohydr. Polym. 83 (2011) 776–786, https://doi.org/10.1016/j.carbpol.2010.08.052.

[45] D. Zhao, J. Sun, Q. Li, G.D. Stucky, Morphological control of highly ordered mesoporous silica SBA-15, Chem. Mater. 12 (2000) 275–279, https://doi.org/10.1021/cm9911363.

[46] M. Thommes, K. Kaneko, A.V. Neimark, J.P. Olivier, F. Rodriguez-Reinoso, J. Rouquerol, K.S.W. Sing, Physisorption of gases, with special reference to the evaluation of surface area and pore size distribution (IUPAC Technical Report), Pure Appl. Chem. 87 (2015) 1051–1069, https://doi.org/10.1515/pac-2014-1117.

[47] Y. Zeng, L. Prasetyo, S.J. Tan, C. Fan, D.D. Do, D. Nicholson, On the hysteresis of adsorption and desorption of simple gases in open end and closed end pores, Chem. Eng. Sci. 158 (2017) 462–479, https://doi.org/10.1016/j.ces.2016.10.048.

[48] C. Gebald, J.A. Wurzbacher, P. Tingaut, T. Zimmermann, A. Steinfeld, Amine-based nanofibrillated cellulose as adsorbent for CO_2 capture from air, Environ. Sci. Technol. 45 (2011) 9101–9108, https://doi.org/10.1021/es202223p.

[49] C.H. Giles, D. Smith, A. Huitson, A general treatment and classification of the solute adsorption isotherm. I. Theoretical, J. Colloid Interface Sci. 47 (1974) 755–765, https://doi.org/10.1016/0021-9797(74)90252-5.

[50] F. Trotta, M. Zanetti, G. Camino, Thermal degradation of cyclodextrins, Polym. Degrad. Stab. 69 (2000) 373–379, https://doi.org/10.1016/S0141-3910(00)00084-7.

[51] M. Colilla, I. Izquierdo-Barba, S. Sánchez-Salcedo, J.L.G. Fierro, J.L. Hueso, M. Vallet-Regí, Synthesis and characterization of zwitterionic SBA-15 nanostructured materials, Chem. Mater. 22 (2010) 6459–6466, https://doi.org/10.1021/cm102827y.

[52] J.M. Rosenholm, M. Lindén, Towards establishing structure-activity relationships for mesoporous silica in drug delivery applications, J. Control. Release Off. J. Control. Release Soc. 128 (2008) 157–164, https://doi.org/10.1016/j.jconrel.2008.02.013.

[53] A. Popat, J. Liu, G.Q. (Max) Lu, S.Z. Qiao, A pH-responsive drug delivery system based on chitosan coated mesoporous silica nanoparticles, J. Mater. Chem. 22 (2012) 11173–11178, https://doi.org/10.1039/C2JM30501A.

[54] J.C. Doadrio, E.M.B. Sousa, I. Izquierdo-Barba, A.L. Doadrio, J. Perez-Pariente, M. Vallet-Regí, Functionalization of mesoporous materials with long alkyl chains as a strategy for controlling drug delivery pattern, J. Mater. Chem. 16 (2006) 462–466, https://doi.org/10.1039/B510101H.

[55] L. Polo, N. Gómez-Cerezo, A. García-Fernández, E. Aznar, J.-L. Vivancos, D. Arcos, M. Vallet-Regí, R. Martínez-Máñez, Mesoporous bioactive glasses equipped with stimuli-responsive molecular gates for controlled delivery of levofloxacin against bacteria, Chem. - Eur. J. (2018), https://doi.org/10.1002/chem.201803301.

[56] S. Pathan, P. Solanki, A. Patel, Functionalized SBA-15 for controlled release of poorly soluble drug, Erythromycin, Micropor. Mesopor. Mater. 258 (2018) 114–121, https://doi.org/10.1016/j.micromeso.2017.09.012.

[57] M. Hamzehloo, J. Karimi, K. Aghapoor, H. Sayahi, H.R. Darabi, The synergistic cooperation between MCM-41 and azithromycin: a pH responsive system for drug adsorption and release, J. Porous Mater. 25 (2018) 1275–1285, https://doi.org/10.1007/s10934-017-0538-3.

[58] J. Anderson, J. Rosenholm, M., Linden, N. Ashammakhi, Mesoporous silica: An alternative diffusion controlled drug delivery system, in: Top. Multifunct. Biomater. Devices, University of Oulund, Finland, 2008: pp. 1–19.

[59] A. Doadrio, A. Salinas, J. Sánchez-Montero, M. Vallet-Regí, Drug release from ordered mesoporous silicas, Curr. Pharm. Des. 21 (2015) 6213–6819, https://doi.org/10.2174/1381612822666151106121419.

[60] S. Tomkova, M. Misuth, L. Lenkavska, P. Miskovsky, V. Huntosova, In vitro identification of mitochondrial oxidative stress production by time-resolved fluorescence imaging of glioma cells, Biochim. Biophys. Acta BBA - Mol. Cell Res. (1865 (2018)) 616–628, https://doi.org/10.1016/j.bbamcr.2018.01.012.

[61] X. Chen, X. Yao, L. Chen, Intracellular pH-sensitive dextran-based micelles as efficient drug delivery platforms, Polym. Int. 64 (2015) 430–436, https://doi.org/10.1002/pi.4809.

[62] X.-Y. Hu, J.-Y. Liang, X.-J. Guo, L. Liu, Y.-B. Guo, 5-Fluorouracil combined with apigenin enhances anticancer activity through mitochondrial membrane potential (ΔΨm)-mediated apoptosis in hepatocellular carcinoma, Clin. Exp. Pharmacol. Physiol. 42 (2015) 146–153, https://doi.org/10.1111/1440-1681.12333.

[63] H. Zhao, Q. Liu, S. Wang, F. Dai, X. Cheng, X. Cheng, W. Chen, M. Zhang, D. Chen, In vitro additive antitumor effects of dimethoxycurcumin and 5-fluorouracil in colon cancer cells, Cancer Med. 6 (2017) 1698–1706, https://doi.org/10.1002/cam4.1114.

[64] L. Scorrano, V. Petronilli, R. Colonna, F.D. Lisa, P. Bernardi, Chloromethyltetramethylrosamine (Mitotracker OrangeTM) Induces the mitochondrial permeability transition and inhibits respiratory complex I implications for the mechanism of cytochrome crelease, J. Biol. Chem. 274 (1999) 24657–24663, https://doi.org/10.1074/jbc.274.35.24657.

[65] S. Kascakova, Z. Nadova, A. Mateasik, J. Mikes, V. Huntosova, M. Refregiers, F. Sureau, J.-C. Maurizot, P. Miskovsky, D. Jancura, High level of low-density lipoprotein receptors enhance hypericin uptake by U-87 MG cells in the presence of LDL, Photochem. Photobiol. 84 (2008) 120–127, https://doi.org/10.1111/j.1751-1097.2007.00207.x.

[66] V. Huntosova, Z. Nadova, L. Dzurova, V. Jakusova, F. Sureau, P. Miskovsky, Cell death response of U87 glioma cells on hypericin photoactivation is mediated by dynamics of hypericin subcellular distribution and its aggregation in cellular organelles, Photochem. Photobiol. Sci. 11 (2012) 1428–1436, https://doi.org/10.1039/C2PP05409D.

[67] D. Patel, S. Shukla, S. Gupta, Apigenin and cancer chemoprevention: Progress, potential and promise (Review), Int. J. Oncol. 30 (2007) 233–245, https://doi.org/10.3892/ijo.30.1.233.

[68] K. Siposova, V. Huntosova, Y. Shlapa, L. Lenkavska, M. Macajova, A. Belous, A. Musatov, Advances in the study of cerium oxide nanoparticles: new insights into antiamyloidogenic activity, ACS Appl. Bio Mater. 2 (2019) 1884–1896, https://doi.org/10.1021/acsabm.8b00816.